Molecular BioSystems

Accepted Manuscript

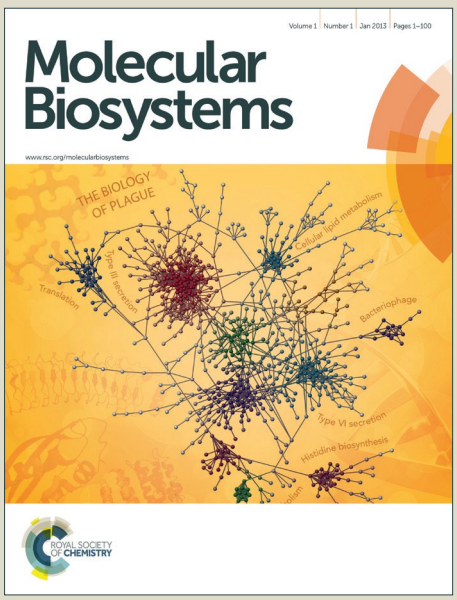

ROYAL SOCIETY OF CHEMISTRY

www.rsc.org/molecularbiosystems

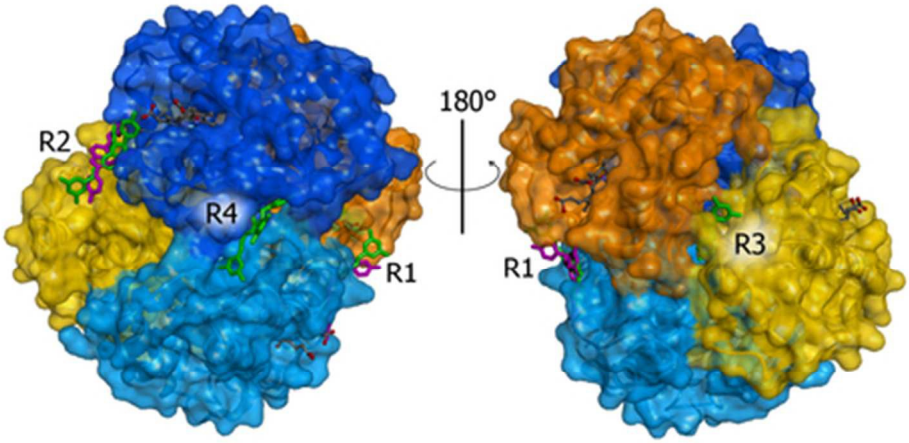

39x21mm (300 x 300 DPI)

Journal Name

ARTICLE

Insights into the properties of the two enantiomers of *trans*-δ-viniferin, a resveratrol derivative: antioxidant activity, biochemical and molecular modeling studies of the interactions with hemoglobin

Received 00th January 20xx,
Accepted 00th January 20xx

DOI: 10.1039/x0xx00000x

www.rsc.org/

Silvana Ficarra[a†], Ester Tellone[a†], Davide Pirolli[b], Annamaria Russo[a], Davide Barreca[a], Antonio Galtieri[a], Bruno Giardina[c], Paolo Gavezzotti[d], Sergio Riva[d] and Maria Cristina De Rosa[c]*

Resveratrol is widely known as an antioxidant and anti-inflammatory molecule. The present study first reports the effects of *trans*-δ-viniferin (TVN), a dimer of resveratrol, on human erythrocytes. The antioxidant activity of TVN was tested using in vitro model systems such as hydroxy radical scavenging, DPPH and lipid peroxidation. In addition we have examined the influence of the 15*R*,22*R*- and 15*S*,22*S*-enantiomers (abbreviated R,R-TVN, and S,S-TVN, respectively) on anion transport, ATP release, caspase 3 activation. Given that hemoglobin (Hb) redox reactions are the major source of RBC oxidative stress, we also explored the effects of TVN on hemoglobin function. TVN showed moderate antioxidant properties and good protective activity from hemoglobin oxidation. Potential binding sites of R,R-TVN and S,S-TVN with oxy- and deoxy-Hb were also investigated through an extensive *in silico* docking approach and molecular dynamics calculations. On the whole molecular modeling studies indicate that binding of R,R-TVN and S,S-TVN to Hb lacks of specific ligand-target interactions. This is the first report on the biological activity of the individual enantiomers of a resveratrol-related dimer.

Introduction

The polyphenol *trans*-resveratrol (*trans*-3,5,4'-trihydroxystilbene), a phytoalexin produced in response to stress, has been the most widely studied stilbene for its role in human health.[1-4] In nature, resveratrol exists in two isomeric forms (*cis* and *trans* configurations of the olefinic bond, the first less biologically active than the second) either as β-glycosylated derivatives, named piceids, or as the aglycone.[5] The antioxidative property of resveratrol is an important aspect of its physiological activity in humans. Bioactive phenols can quench reactive oxidative species (ROS), such as hydrogen peroxide, superoxide and the hydroxyl radical, thus avoiding pro-oxidative damages in humans.[6]

Furthermore, recent studies have revealed that resveratrol is able to cross the erythrocyte membrane, interact with haemoglobin, modulate the red blood cell metabolism and exert a protective role in several neurodegenerative diseases.[7,8]

Stilbenes are also known to occur in oligomeric forms and their biosynthesis includes an oxidative polymerization of the monomer resveratrol by peroxidases.[9] Langcake and Pryce have identified oxidation products of resveratrol such as ε-, α-, β- and γ-viniferin, which are dimer, trimer, tetramer and a more highly polymerized oligomer, respectively.[10] Some of these oligomers have been tested for their antioxidant properties and, among them, *trans*-ε-viniferin has been the subject of several studies.[11–15]

[a]*Department of Chemical, Biological, Pharmaceutical and Environmental Sciences University of Messina, V.le F. Stagno d'Alcontres 31, 98166 Messina, Italy*
[b]*Istituto di Biochimica e Biochimica Clinica, Università Cattolica del Sacro Cuore L.go F. Vito 1, 00168 Rome, Italy*
[c]*Istituto di Chimica del Riconoscimento Molecolare (ICRM) - CNR c/o Università Cattolica del Sacro Cuore L.go F. Vito 1, 00168 Rome, Italy*
[d]*Istituto di Chimica del Riconoscimento Molecolare (ICRM - CNR., via Mario Bianco 9, 20131 Milano, Italy*
† Co-first author
* Corresponding author

Trans-δ-viniferin (TVN) is another resveratrol dimer isolated from grapes in response to fungal infection.[16-18] It was shown to be one of the major stilbenes synthesized by *Plasmopora viticola*-infected grapevine leaves and to exhibit inhibitory activity against cyclooxygenase-1 and -2.[19,20] However, despite the fact that several biochemical and biophysical studies have been performed, information on the antioxidative activity of *trans*-δ-viniferin in humans is still limited.[21,22]

The aim of the present investigation was to evaluate the biological activity of TVN and of its (15*R*, 22*R*)- and (15*S*, 22*S*) enantiomers (abbreviated as R,R-TVN and S,S-TVN, Figure 1). In this context, a new reliable and easily scalable approach for the isolation of the enantiomerically pure R,R-TVN and S,S-TVN has been recently developed, exploiting a sequential combination of biocatalyzed reactions (laccase-catalyzed oxidation, β-glucosidases-catalyzed hydrolysis) and chromatographic separations with a semi-preparative HPLC chiral column.[23] Preliminary evaluation of the radical scavenger activities using the DPPH reduction method showed that *trans*-δ-viniferin has a higher IC50 value ($9.5 \cdot 10^{-4}$ mmol/ml) with respect to resveratrol ($6.1 \cdot 10^{-5}$ mmol/ml).[24]

In this study we have sought to evaluate the antioxidant profile of *trans*-δ-viniferin using different assays or methodologies, given that the use of a single method for the measurement of antioxidant activity can yield results which are not reproducible by other antioxidant methods.[25] It is worthwhile to remember that methods of measuring antioxidant activity are extremely dependent on the conditions used and on the substrates or products monitored. The methods we have used to measure the total antioxidant capacity were FRAP (ferric reducing/antioxidant power), DPPH (2,2-diphenyl-1-picrylhydrazyl) and nitrite-induced hemoglobin oxidation. The scavenging activities of hydroxyl radicals and lipid peroxidation inhibition capacity have also been evaluated.

Moreover, the biological activities of R,R-TVN and S,S-TVN have been investigated in vitro on human erythrocytes (RBC, red blood cell) which, due to the presence of only a single membrane and the lack of internal organelles, constitute an ideal cell system for studying basic drug-biomembrane interactions.[26,27] The effect of the two enantiomers on the RBC membrane functionality (anion transport, ATP release) and on the interaction with cytosolic proteins (hemoglobin and caspase 3) has been assessed.

Computational modeling, with its ability to assess the protein-ligand interactions at atomic level, has been increasingly employed to explore the structural properties of biomolecular complexes.[28,29] To provide a structural basis for the observed interaction of *trans*-δ-viniferin with human hemoglobin (Hb) we have complemented the experimental investigation by using molecular docking and molecular dynamics simulation, in an effort aimed to elucidate the biochemical mechanisms of activities of these bioactive compounds.

Experimental

Materials and methods

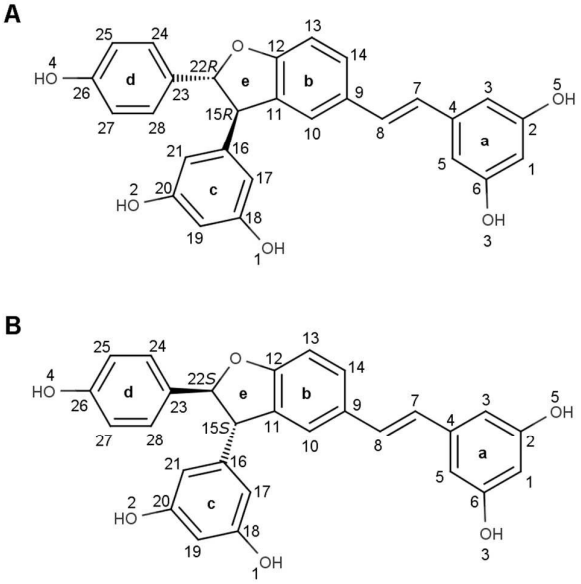

Figure 1. Chemical structures of 15*R*,22*R*-*trans*-δ-viniferin (R,R-TVN) (A) and 15*S*,22*S*-*trans*-δ-viniferin (S,S-TVN) (B) with numbering according to Mikulski & Molski.[22]

All biochemical reagents were purchased from Sigma-Aldrich (St. Louis, MO, USA). Racemic TVN, R,R-TVN and S,S-TVN were prepared as described.[23] Citrate fresh human blood was obtained from informed healthy donors under the declaration that they had avoided any drug treatment for at least one week prior to sample collection, in accordance with the principles outlined in the Declaration of Helsinki.

Limit of detection, applicability and interpretation are in agreement with those reported in the cited references of this section.

Preparation of red blood cells

Citrate blood samples were washed three times with an isosmotic NaCl solution. During washing, the white blood cells were discarded from the pellet. After washing, the RBCs were resuspended (hematocrit 4%) in the incubation buffer (35 mM Na_2SO_4, 90 mM NaCl, 25 mM N-(2-hydroxyethyl)-piperazine-N1-2-ethanesulfonic acid (HEPES), 1.5 mM $MgCl_2$) adjusted to pH 7.4 and with a value of 310 ± 20 mOsmol/kg, measured by an Osmostat OM-6020 apparatus (Daiichikagakuco, Kyoto, Japan).

HPLC determinations

Washed RBCs were incubated at 37°C for 2 h with 50 μM R,R-TVN and S,S-TVN, respectively. Samples were washed and the packed cells were lysed with 10% ethanol. Lysates were centrifuged for 10 min at 4000 x g (4°C) and the supernatant was filtered with 0.45 mm filter. Free R,R-TVN and S,S-TVN were analyzed by HPLC with a Shimadzu system, consisting of an LC-10AD pomp system and an SPDM10A diode array detector, a Rheodyne 7725i injector with a 20 ml sample loop and a reverse-phase Supelco C18 column (5 mm, 250 x 4.6

mm). The mobile phase consisted of a linear gradient of acetonitrile in H_2O as follows: 5–20% (0–2 min), 20–30% (2–4 min), 30-100% (4–7 min), 100% (7–10 min). The flow rate was 1.0 ml/min at 25°C. R,R-TVN and S,S-TVN were detected at 320 nm and determined by comparison of peak areas with a standard solution of 50 μM of R,R-TVN and S,S-TVN. Binding of R,R-TVN and S,S-TVN to Hb was analyzed by HPLC as described above. Purified Hb (0.7 mg/ml) in the T or R state, was incubated for 15 min in $1{\cdot}10^{-1}$ M HEPES buffer plus $1{\cdot}10^{-1}$ M NaCl with 50 μM R,R-TVN and S,S-TVN and $3{\cdot}10^{-3}$ M 2,3-bisphosphoglycerate at pH 7.4.

Sulphate transport measurement

Washed RBCs were incubated in a buffer containing sulphate at 25 °C in the presence and absence of 50μM TVN, R,R-TVN and S,S-TVN. At specified intervals 10 μmol of 4-acetamido-4′-isothiocyanostilbene-2,2′-disulfonic acid (SITS) stopping medium was added to each test tube containing the RBC suspension. Cells were separated from the incubation medium by centrifugation (J2-HS Centrifuge, Beckman, Palo Alto, CA, USA) and washed three times at 4 °C with a sulphate-free medium. After the final washing, the packed cells were lysed with perchloric acid (4%) and distilled water and centrifuged at 4 °C. Sulphate ions in the supernatant were precipitated by adding glycerol and distilled water (1:1), 4 M NaCl and 1 M HCl solution, and 1.23 M $BaCl_2.2H_2O$ to obtain a homogeneous barium sulphate precipitate. The intracellular sulphate concentration was measured by spectrophotometry at 425 nm wavelength as previously reported.[30]

Measurement of ATP

Erythrocytes were incubated with R,R-TVN or S,S-TVN 50 μM and ATP was measured by the luciferin–luciferase technique as previously reported, with minor modifications.[7,31]

Caspase 3 activity assay

Erythrocytes were incubated in the absence or in the presence of 25 and 50 μM TVN, R,R-TVN and S,S-TVN or t-butyl hydroperoxide (t-BHT) 100 μM for 2 h at 37°C and Caspase 3 activity was determined as previously reported.[32]

Hydroxyl radical scavenging

Hydroxyl radical scavenging was assayed as described by Halliwell, with slight modifications.[33] This assay is based on quantification of the degradation product of 2-deoxyribose by condensation with thiobarbituric acid (TBA). The reaction mixture contains 2.8 mM 2-deoxy-2-ribose, 10 mM phosphate buffer pH 7.4, 25 μM $FeCl_3$, 100 μM EDTA, 2.8 mM H_2O_2, 100 μM ascorbic acid and different concentrations of TVN (0–100 μM) in a final volume of 1 ml. The samples were incubated for 1 h at 37 °C in a water bath. After cooling, the absorbance was measured at 532 nm against an appropriate blank solution.

Lipid peroxidation assay

Isolated erythrocytes were incubated for 2 h in the absence or in the presence of TVN and t-BHT (100 μM), as previously reported.[34] Assay for lipid peroxidation was performed using the thiobarbituric acid reactive substances (TBARS).

Metal chelating activity

The ability of TVN to chelate ferrous ions was measured according to the method described by Dinis et al.[35] Different concentrations (0-100 μM) of TVN were added to a solution of 20 μM $FeCl_2$ to measure chelating activity of ferrous ions. The inhibition percentage of ferrozine-Fe^{2+} complex formation was calculated as $[(A_0-A_s)/A_0]x100$, where A_0 was the absorbance of the control, and As was the absorbance of the samples in the presence of the analysed compounds.

Ferric reducing antioxidant power (FRAP)

The FRAP assay was performed according to Benzie & Strain with minor modification.[36] The test determines the ferric reducing ability of plasma (FRAP) by using antioxidants as reductants in a redox-linked colorimetric method. The purpose of the FRAP assay is to detect a change in absorption when the ferric form of iron (Fe^{3+}) reduces to ferrous form (Fe^{2+}) (emitting a strong blue color; Fe^{2+}/2,4,6-Tris(2-pyridyl)-S-triazine (TPTZ)), representing the reducing power of electron-donating antioxidants within the plasma reaction mixture. The fresh working FRAP reagent was prepared daily by mixing 25 ml of acetate buffer (300 mM, pH 3.6), 2.5 ml of TPTZ solution (10 mM in 40 mM HCl) and 2.5 ml of $FeCl_3.6H_2O$ solution (20 mM). The reagent was warmed to 37 °C; then 1500 μl were placed in a cuvette (1.0 cm path length) and the initial absorbance was read. A 50 μl volume of TVN solution was added to the cuvette and the absorbance was measured after 4 min at wavelength 593 nm. The final concentration of the tested compounds ranged from 0 to 100 μM.

DPPH (2,2-Diphenyl-1-picrylhydrazyl) assay

The free radical scavenging effect of tested compounds was assessed by the free radical method as previously reported using the stable free radical 2,2-diphenyl-1-picrylhydrazyl (DPPH) which forms a violet solution and reacts with antioxidants losing its color.[37] The color loss and subsequent fall in absorbance is correlated to the antioxidant content of the sample. Test compounds at a concentrations ranging from 0 to 250 μM, in a final volume of 3.0 ml, were mixed with 80 μM $DPPH^{\cdot}$ in methanol. The changes in absorbance at 517 nm were monitored over 30 min. $DPPH^{\cdot}$ concentration in the cuvette was chosen to give absorbance values less than 1.0.

Effect of R,R-TVN and S,S-TVN on the time course of nitrite-induced oxidation of Hb

In vitro model for oxidation of Hb with sodium nitrite was utilized for production of methemoglobin (metHb). The purified Hb, suspended in Hepes buffer was incubated in the absence (control) and in presence of 50 μM of R,R-TVN or S,S-TVN and concomitantly 0.3 mM $NaNO_2$. The formation of

metHb was monitored spectrophotometrically at 1 minute intervals for a total of 20 minutes using a spectrophotometer UV-visible Beckman DU640.

Molecular docking of R,R-TVN and S,S-TVN with HbA

The binding modes of R,R-TVN and S,S-TVN, on the oxygenated (R) and deoxygenated (T) states of hemoglobin, were studied using docking simulations.[38] Blind docking, in which no assumptions were made concerning where within hemoglobin R,R-TVN and S,S-TVN might be expected to bind, was performed with Autodock 4.2, a widely-used grid-based docking program known for its accuracy.[39-41] The blind docking protocol was developed and validated by redocking a co-crystallized ligand of carboxyhemoglobin, di(5-(2,3-dihydro-1,4-benzodioxin-2-yl)-4H-1,2,4-triazol-3-yl)disulfide (TD-1), with its corresponding crystal structure (PDB ID code: 4NI1).[42] The docked conformation of the ligand had root mean square deviation (rmsd) value of 2.5 Å with the experimental TD-1 structure.[43] The R,R-TVN and S,S-TVN stereoisomers were built starting from the crystallographic structure of *trans*-resveratrol (PDB ID: 1DVS) and using the sketch module available within DiscoveryStudio 4.0 suite of programs (Biovia, San Diego, CA).[44] The molecular geometry was optimized by energy minimization using CHARMm force field and restraining the stilbene moiety to planarity.[45] For T and R states of Hb, the crystallographic structures of deoxygenated and oxygenated human haemoglobin were obtained from the Protein Data Bank, PDB ID codes: 2DN2 and 2DN1, respectively.[46] AutoDockTools (ADT) was used to add polar hydrogens and partial charges for proteins and ligands using the Kollman United Atom and Gasteiger charges, respectively. The ligand has nine rotable bonds (C2–O5, C6–O3, C7-C4, C8-C9, C15–C16, C22–C23, C26-O4, C20-O2, C18-O1), while the protein was fixed in geometry. During the blind docking process, the search was extended over the whole receptor protein without imposing the binding site, using cubic grid fields with grid points separated by 0.335 Å. The maximum number of energy evaluations and the maximum number of generations were set to $2.5 \cdot 10^6$ and 27000, respectively for each run. 2000 LGA (Lamarckian genetic algorithm) runs were conducted for each template and the resulting docked conformations were clustered into groups of similar binding modes, with a root mean square deviation (rmsd) of 3.0 Å using AutoDockTools. In a second step, we docked the ligands in each of the binding sites found in the first step ("refined docking") using two different docking programs, AutoDock and Glide Extra Precision (XP) (Schrodinger Suite).[47] This time, the grid field was a 20 Å cube centered on the best scored conformation obtained in the first step and 150 LGA runs were conducted for each template. In the case of Glide, protein coordinates were preprocessed for docking using the Protein Preparation Wizard provided in the Schrodinger Maestro environment, whereas ligands were prepared for docking using the LigPrep process.

Molecular dynamics calculations

All obtained docking solutions from the refined docking simulations were submitted to aqueous-phase molecular dynamics (MD) simulations. MD and analysis of the trajectories were carried out employing GROMACS 4.6.7 and the GROMOS96 53a6 force field.[48,49] The parameters for the topology of the ligands were obtained using the Automated Topology Builder (ATB) server. For the purpose of comparison, MD simulations on the unbound deoxyHb and oxyHb structures were also performed. Each simulated system was embedded in a triclinic box, filled with explicit SPC/E water molecules and then neutralized by 6 Na^+ counter ions that were added at random positions to the bulk solvent. The box dimensions (8.43 nm x 7.52 nm × 7.68 nm) were set to allow at least 0.9 nm between the protein and the box faces on each side. The systems were first minimized and then equilibrated under NVT conditions for 100 ps at 300 K, followed by 100 ps under NPT conditions, applying position restraints to the protein and ligand atoms. Finally, all restraints were removed and 14 MD simulations were run for 10 ns at 300 K. A cut-off of 1.2 Å was used for the short-range electrostatic and van der Waals interactions. Long-range electrostatic interactions were calculated using Particle Mesh Ewald method.[50] The Linear Constraint Solver (LINCS), which removes the fastest degrees of freedom by applying holonomic constraints to the covalent bonds and allows to employ a larger timestep of 0.002 ps during the simulation, was used.[51] Coordinates and energies were saved every 2 ps for analysis which was carried out using the standard GROMACS tools, such as g_rmsf and g_rms.
All computations were carried out on a CentOS 5 Linux operating system, running on HP Z820 workstations with Intel® Xeon® E5-2620 (2.00GH) cpu and graphical processing unit (GPU) NVIDIA Quadro 2000.

Statistical Analysis

Data are presented as mean of at least three independent experiments ± standard deviation (SD). Data were analyzed by one-way analysis of variance. Significance was calculated by Student's t-test.

Results and discussion

Antioxidant properties of *trans*-δ-viniferin

The antioxidant properties of *trans*-δ-viniferin (TVN) have been evaluated using different assays (Fig. 2). Among the oxygen radicals, the hydroxyl radical is the most reactive and causes great damage to living cells due to its ability to react with various molecules such as phospholipids, DNA, and organic acids. The ability of *trans*-ε-viniferin and cis-ε-viniferin to scavenge the hydroxyl radicals was previously determined in the deoxyribose degradation test.[12]
The effect of increasing concentrations (up to 100 μM) of our racemic *trans*-δ-viniferin on deoxyribose damage

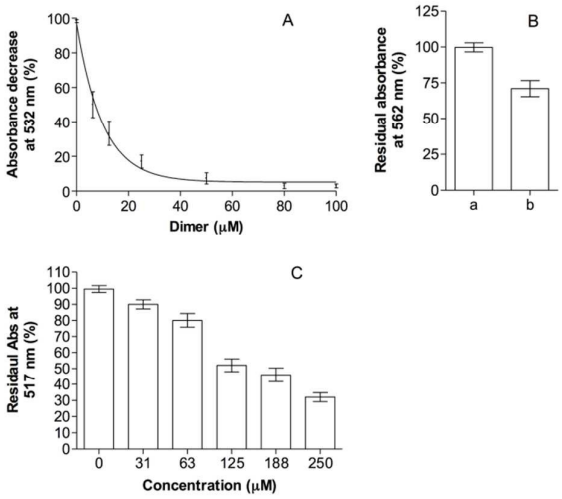

Figure 2. Antioxidant activity of *trans*-δ-viniferin (TVN). Deoxyribose (A), ferrous ion chelating (B) and DPPH (C) assays of TVN. Results for TVN (a) in B panel are reported in comparison with the blank control (b).

induced by Fe^{3+}/H_2O_2, as described by Halliwell in reference 33, is reported in Figure 2A. The molecule exhibited quenching ability against hydroxyl radicals showing a degree of OH· inhibition of about ~58% at a concentration of 10 μM (Fig. 2A). The obtained IC_{50} value for the compound, 7.3±0.3 μM, exhibited an antioxidative activity that was weaker with respect to *trans*-ε- viniferin but equal to that exerted by *trans* resveratrol (0.17 and 7.35 μM, respectively).[52]

The hydroxyl radical is considered one of the fast initiators of the lipid peroxidation process.[53] The protection against lipid peroxidation was estimated by dosing the inhibition of thiobarbituric acid reactive substance. Notably, *trans*-δ-viniferin did not inhibit lipid peroxidation (data not shown). As previously reported by others, these results confirm that the free radical scavenging capacity and the efficacy for inhibition of lipid peroxidation do not always match.[54–56]

Ferrous ion is a key transition metal responsible for initiation of peroxidation in biological systems. Chelating agents reduce the concentration of metal ions available for catalyzing peroxidation and thus are known to serve as effective secondary antioxidants. As described by Dinis et al., ferrous ions form a complex with ferrozine, and the intensity of the purple colour of the complex decreases in the presence of chelating agents.[35] The amount of iron chelated by *trans*-δ-viniferin (100 μM), calculated by difference in absorbance between a blank (Fe^{2+}-ferrozine) and a sample (Fe^{2+}-ferrozine and *trans*-δ-viniferin), is shown in Fig. 2B indicating that the chelating ability of the compound was about 30%.

The reducing power and the antiradical properties of the samples were then assessed using FRAP and DPPH assays, respectively. The FRAP assay is based on the measurement of the ability of a substance to reduce Fe(III) to Fe(II); the greater the reducing ability, the better the antioxidant property. Antioxidants may reduce the colourless Fe(III)-TPTZ to a blue Fe(II)-TPTZ complex, which results in an increase in the absorbance at 595 nm, giving the so called FRAP value. The FRAP values of increasing concentrations of *trans*-δ-viniferin showed no significant iron reducing activity (data not shown). In the DPPH assay, the decrease of absorbance is correlated with the antioxidant potency of the compounds. DPPH· is a stable free radical containing an odd electron in its structure and is used for detecting radical scavenging activity. The degree of decrease in the absorbance of DPPH indicates the free-radical scavenging potentials. The free radical scavenging capacities of *trans*-δ-viniferin is shown in Figure 2C with an efficiency of about 50% at concentration higher than 100 μM. These results showed that the antioxidant activity of TVN is basically due to radical-scavenging effects rather than to a reducing activity. These findings are in agreement and somehow confirm previous investigations on resveratrol moderate antioxidant activity towards the DPPH radical.[57–59]

The interaction of *trans*-δ-viniferin and its enantiomers with haemoglobin

Both the racemic mixture and the R,R-TVN, S,S-TVN enantiomers easily cross RBC membrane by means of passive diffusion.[60] RBC concentration of *trans*-δ-viniferin was assayed using a high performance liquid chromatographic method. The study showed that the majority of racemate (~90%), S,S-TVN (~80%) and R,R-TVN (~60%) was present inside the RBC. Different types of drug interactions with proteins in RBCs have been observed and many of them involve Hb, which accounts for 95%-97% of the cytosolic protein.[61] The observed significant levels of the two enantiomers and high intraerythrocytic concentration of Hb suggest a potential interaction between the tested compounds and the protein.[62]

To find evidence to support the interaction between *trans*-δ-viniferin and Hb, additional studies using HPLC analysis were performed on purified oxy- and deoxy-Hb incubated with the racemic TVN, R,R-TVN and S,S-TVN, respectively. Our findings indicate that all the tested compounds interact with Hb, but to a different extent and that, as already observed for resveratrol the observed binding is oxygen dependent (Fig. 3).[7,59] S,S-TVN appears to interact more tightly with Hb than R,R-TVN and, in general, the two enantiomers interact more favorably with the deoxy form. The levels of free *trans*-δ-viniferin were 50% (R,R-TVN) and 40% (S,S-TVN) of the total amount in the oxygenated solution, 40% (R,R-TVN) and 20% (S,S-TVN) in the deoxygenated one (Fig. 3A,B).

Molecular modelling of R,R-TVN and S,S-TVN into oxy- and deoxy-Hb

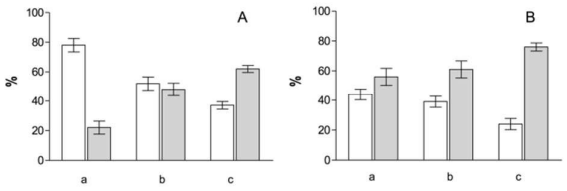

Figure 3. HPLC measurements of the amount of *trans*-δ-viniferin (TVN) free (white bars) or bound (grey bars) in the oxygenated (A) and deoxygenated (B) state of protein. (a) TVN, (b), R,R-TVN and (c) S,S-TVN. Conditions: purified Hb (0.7 mg/ml) was incubated with 50 μM of TVN, R,R-TVN and S,S-TVN, respectively.

To investigate the potential sites for R,R-TVN and S,S-TVN binding in oxy- (R state) and deoxy- (T state) Hb, we carried out *in silico* molecular docking studies. Blind docking is commonly used to generate protein-ligand complexes when a binding site is undetermined.[63,64] Blind docking simulations of R,R-TVN and S,S-TVN were performed with AutoDock scanning the entire surface of oxy- and deoxy-Hb. In the case of R,R-TVN 2000 docking conformations were grouped into 41 (oxy-Hb) and 33 (deoxy-Hb) clusters whereas docking analysis of the S,S-TVN ligand produced 30 and 18 different clusters on oxy-Hb and deoxy-Hb, respectively. This result reflects the high number of rotatable bonds in the two enantiomers that make it difficult to find the best binding mode.

A large number of clusters, in fact, implies existence of a wide range of binding modes and lack of specific ligand-target interactions. Several studies show that the most populated clusters of the docked ligand conformations are better predictors of the native binding mode.[65,66] The majority of the results concerning molecular docking are shown in Table 1 and the location of the most populated clusters is shown in Figure 4. Two large clusters emerged from the blind docking of R,R-TVN in oxy-Hb. One of these contains 405 orientations, the best one with a score of -7.79 kcal/mol and is located at the $\alpha_1\beta_2$ interface of the protein (region 1, R1), the cooperative inter-dimeric interface of the protein (Fig. 4A). The other cluster (395 orientations, -7.82 kcal/mol) covers the $\alpha_2\beta_1$ interface (region 2, R2), the symmetrically oriented region of the protein which is arranged as a dimer of identical αβ dimers, possessing two-fold symmetry (Fig. 4A).

In the case of S,S-TVN four large clusters were identified. The most populated one (330 orientations, -7.66 kcal/mol) fits into region 1, R1 (Fig. 4A), the second (307 orientations, -8.43 kcal/mol) was found at the entrance of the central cavity between the two α subunits of the protein (region 3, R3), the third (299 orientations, -7.01 kcal) is located at the entrance of the central cavity between the two β subunits (region 4, R4), the fourth (286 orientations, -7.68 kcal/mol) fits into region 2 (Fig. 4A).

Four clusters were identified by the docking analysis of R,R-TVN with deoxy-Hb (Fig. 4B). The first cluster (400

Table 1. Results of blind docking

	binding energy (kcal/mol)	number in cluster	site
RR-TVN/oxy-Hb			
R1	-7.79	405	$\alpha_1\beta_2$
R2	-7.82	395	$\alpha_2\beta_1$
SS-TVN/oxy-Hb			
R1	-7.66	330	$\alpha_1\beta_2$
R3	-8.43	307	$\alpha_1\alpha_2$
R4	-7.01	299	$\beta_1\beta_2$
R2	-7.68	286	$\alpha_2\beta_1$
RR-TVN/deoxy-Hb			
R1'	-6.86	400	$\alpha_1\alpha_2\beta_2$
R2'	-6.80	388	$\beta_1\beta_2\alpha_2$
R1'	-6.36	314	$\alpha_1\alpha_2\beta_2$
R3'	-7.45	298	$\alpha_1\alpha_2\beta_1$
SS-TVN/deoxy-Hb			
R2'	-6.49	793	$\beta_1\beta_2\alpha_2$
R1'	-8.83	668	$\alpha_1\alpha_2\beta_2$

orientations, -6.86 kcal/mol) is located in the intersubunit cavity between α_1, α_2, and β_2 chains (region 1', R1'), the second cluster (388 orientations, -6.80 kcal/mol) appears in the intersubunit cavity delimited by β_1, β_2, and α_2 chains (region 2', R2'), the third cluster (314 orientations, -6.36 kcal/mol) fits into region 1', whereas the fourth cluster (298 orientations, -7.45 kcal/mol), placed between α_1, α_2, and β_1 subunits (region 3') is symmetrically positioned with respect to the first one (Fig. 4B).

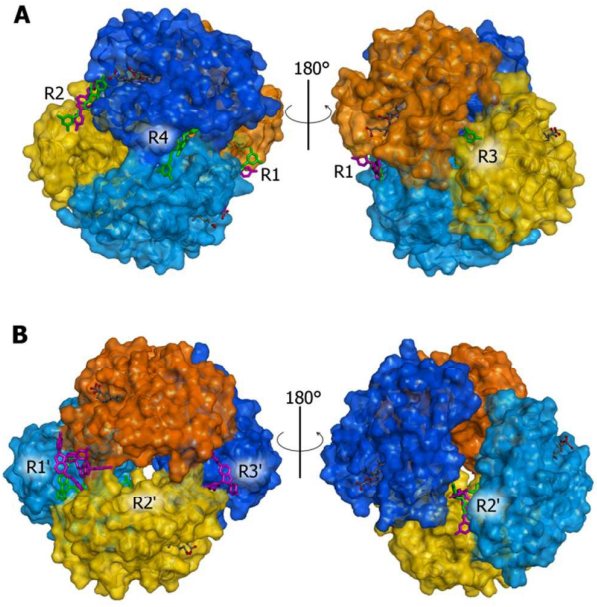

Figure 4. Illustration of the predicted binding sites between R,R-TVN (magenta) and S,S-TVN (green) with oxy (A) and deoxy (B) Hb. The representative poses of the most populated clusters are shown. Orange, α_1; dark blue, β_1; yellow, α_2; light blue, β_2. The heme groups are represented as ball and sticks colored by atom type.

Table 2. Docking scores obtained from AutoDock and Glide

Complexes	Region	Site	Docking Score (kcal/mol)	
			AutoDock	*Glide*
R,R-TVN/oxy-Hb	R1	$\alpha_1\beta_2$	**-8.41**	**-6.743**
	R2	$\alpha_2\beta_1$	-8.09	-6.109
S,S-TVN/ oxy-Hb	R1	$\alpha_1\beta_2$	-7.74	-4.223
	R3	$\alpha_1\alpha_2$	-8.46	-6.456
	R4	$\beta_1\beta_2$	**-8.84**	**-6.640**
	R2	$\alpha_2\beta_1$	-7.73	-3.187
R,R-TVN/deoxy-Hb	R1'	$\alpha_1\alpha_2\beta_2$	-7.79	-6.290
	R2'	$\beta_1\beta_2\alpha_2$	-7.44	-5.612
	R1'	$\alpha_1\alpha_2\beta_2$	-6.68	-5.441
	R3'	$\alpha_1\alpha_2\beta_1$	**-8.24**	**-7.186**
S,S-TVN/deoxy-Hb	R2'	$\beta_1\beta_2\alpha_2$	-7.87	-6.032
	R1'	$\alpha_1\alpha_2\beta_2$	**-9.01**	**-6.316**

In the case of S,S-TVN/deoxy-Hb combination, two large clusters were identified. The most populated of the two (793 orientations, -6.49 kcal/mol) identifies region R2', and the other (668 orientations, -8.83 kcal/mol) is located into region R1' (Fig. 4B). In summary, four and three distinct pockets were identified by *trans*-δ-viniferin as putative binding sites in oxy-Hb and deoxy-Hb, respectively.

To better characterize the possible binding modes of the two enantiomers in each of these regions all the sites predicted by the blind docking were further investigated with a subsequent refined docking step. To this aim, two different docking programs were used, AutoDock and Glide Extra Precision (XP) which use different types of scoring functions and searching methods. Table 2 shows the docking scores obtained from the two docking methods used and reveals, for each binding region, an agreement between the ranking of the docked complexes. However it is worthwhile to notice that the calculated binding energy differences between R,R-TVN and S,S-TVN are small in magnitude when compared to the estimated standard error of the methods (2.5 kcal/mol estimate for the error in the AutoDock binding energy).

On the whole, docking calculations indicate the lack of specific ligand-target interactions and suggest the existence of a wide range of binding modes for *trans*-δ-viniferin to Hb. The analysis of the intermolecular interactions including hydrophobic and hydrogen-bonding contacts was carried out using the LIGPLOT program.[67] Intermolecular interactions in the lowest energy poses, as generated by both AutoDock and Glide (Table 2), are shown in Figure 5 where hydrophobic contacts and hydrogen bonds for oxy- and deoxy-Hb, respectively, are highlighted.

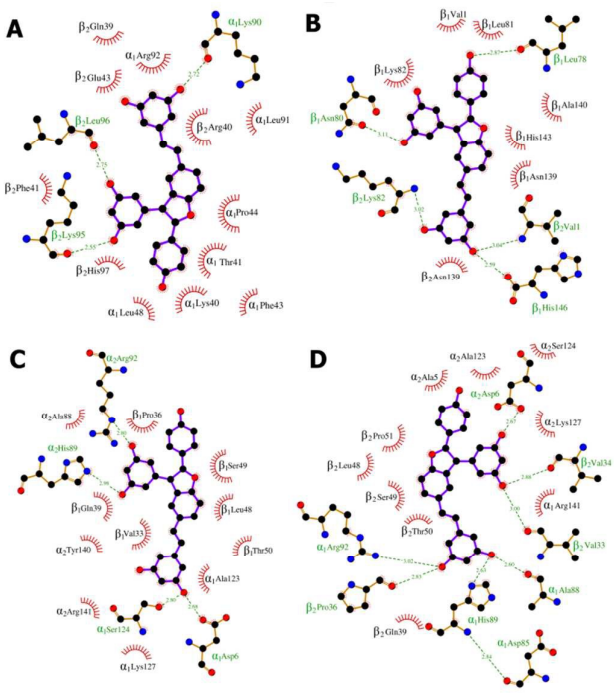

Figure 5. LigPlot analysis results. Diagrams of the lowest energy binding modes (Table 2) of oxy- Hb with R,R-TVN (A) and S,S-TVN (B) and deoxy-Hb with R,R-TVN (C) and S,S-TVN (D) showing the amino acid residues interacting with the substrates through hydrogen bonding and hydrophobic interactions. The green dashed lines correspond to the hydrogen bonds. Spoked arcs represent hydrophobic contacts.

To confirm the docking results and to validate the stability of predicted complexes, the major docking solutions (Table 2), as well as the unbound oxy- and deoxy-Hb structures, were chosen for MD simulation in the presence of explicit solvent. To check the stability of the simulations, the protein Cα-RMSD, the radius of gyration and the ligand Solvent Accessible Surface Area (SASA total) were calculated over the course of simulations and are presented in Table 3. In addition, interactions formed by Hb and *trans*-δ-viniferin were probed by computing the number of hydrogen bonds (HBs) and atomic contacts along the MD simulations. The hydrogen bonding between the predicted ligand–protein structures as a function of simulation time has been presented

Table 3. Time averaged structural properties during MD simulations calculated for the predicted complexes and the unbound proteins (standard deviations are given in parentheses)

System	Cα-RMSD (nm)	Radius of gyration (nm)	Ligand SASA (nm^2)
Oxy-Hb	0.21(0.01)	2.37(0.01)	-
RR-TVN/oxy-Hb			
R1	0.24(0.01)	2.37(0.01)	3.30(0.35)
R2	0.19(0.03)	2.38(0.01)	2.92(0.49)
S,S-TVN/oxy-Hb			
R1	0.21(0.02)	2.35(0.02)	2.95(0.33)
R3	0.21(0.02)	2.36(0.01)	1.76(0.29)
R4	0.22(0.02)	2.37(0.01)	2.48(0.37)
R2	0.22(0.03)	2.36(0.01)	3.97(0.45)
Deoxy-Hb	0.26(0.03)	2.39(0.01)	-
R,R-TVN/deoxy-Hb			
R1’	0.27(0.04)	2.42(0.01)	2.95(0.33)
R2’	0.23(0.04)	2.41(0.01)	2.92(0.49)
R1’	0.24(0.04)	2.39(0.02)	1.76(0.29)
R3’	0.21(0.01)	2.40(0.01)	2.06(0.47)
S,S-TVN/deoxy-Hb			
R2’	0.29(0.04)	2.37(0.01)	3.97(0.45)
R1’	0.35 (0.02)	2.39(0.01)	2.41(0.50)

in Fig. 6. In the potential complexes all the original hydrogen bonds were maintained during the simulation process (Fig. 6). Analysis of the total number of contacts as a function of simulation time (Fig. 7) suggests that, in the predicted complexes, interactions of R,R-TVN and S,S-TVN with oxy- and deoxy-Hb have generally equilibrated within 100 ps. Once bound, the ligand remained attached to the protein even if the simulation was extended to 10 ns (Fig. 7). Results of MD simulation verified the stability of the docked complex and further corroborate the hypothesis that multiple binding sites may exist for both enantiomers of *trans*-δ-viniferin in Hb.

Inhibition of nitrite-induced methemoglobin formation

Nitrite causes a rapid oxidation of hemoglobin to methemoglobin (metHb).[68,69] and superoxide has been implicated in the autocatalytic stage of the oxidation.[70] We evaluated the efficiency of *trans*-δ-viniferin as scavenger of superoxide ascertaining its ability to inhibit nitrite-induced oxidation of hemoglobin to metHb. In the presence of the racemic TVN, R,R-TVN and S,S-TVN, the oxidation process was strongly inhibited. The time required to convert 50% of the available hemoglobin to metHb was 9 min in the absence of the tested compounds, whereas in the presence of the racemic TVN, R,R-TVN and S,S-TVN the formation of metHb was inhibited to a great extent (92.3%±2.0, 71.5%±3.2 and 84.4%±3.1, respectively). Figure 8 shows the effect of TVN on the time course of oxidation of hemoglobin and highlights that the racemic TVN as well as its enantiomers R,R-TVN, S,S-TVN exert a protective function.

Effects of R,R-TVN and S,S-TVN on the erythrocyte membrane

ATP release and anion exchange through erythrocyte membrane are strictly related to Hb saturation with oxygen and to oxidative stress and are often selected as parameters indicative of RBC function and integrity.[31,71,72] It is known that RBCs release ATP when they are deformed or under hypoxic conditions.[73,74]

Examination of the erythrocytes incubated with the racemic TVN, R,R-TVN, S,S-TVN, respectively, and, for comparison, with Mastoparan 7 (Mas 7), a direct activator of the heterotrimeric

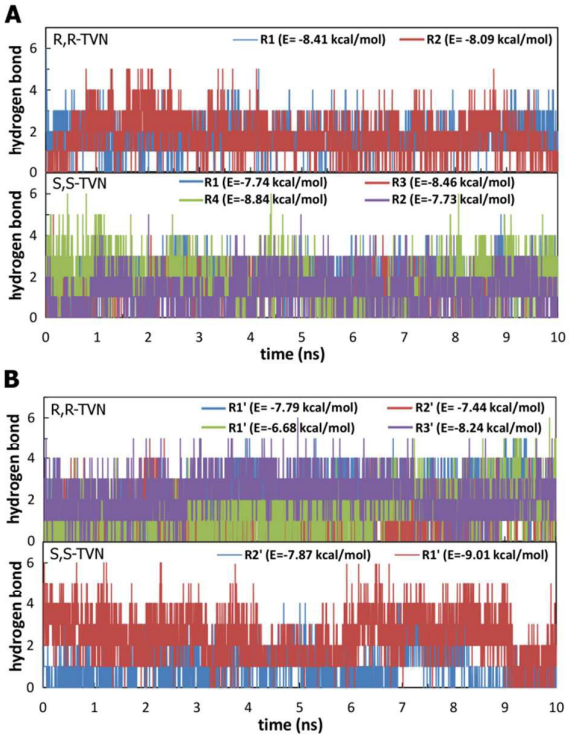

Figure 6. Intermolecular hydrogen bonds (H-bonds). Analysis of total number of intermolecular H-bonds formed between oxy-Hb (A) and deoxy-Hb (B) in the predicted docking complexes as a function of time along the MD simulations. Note the stable number of H-bonds in the generated models.

G protein, indicated that both R,R-TVN and S,S-TVN decreased the release of ATP from RBCs (Figure 9A). In particular, R,R-TVN was able to inhibit the ATP release by 55%, S,S-TVN by 35% and the racemic mixture by 40% (Figure 9A). Different ATP values suggest a different modulation exerted by each enantiomer on cystic fibrosis transmembrane conductance regulator (CFTR). The reduced ATP release might partially offset the increase of the glycolytic pathway (at the expense of

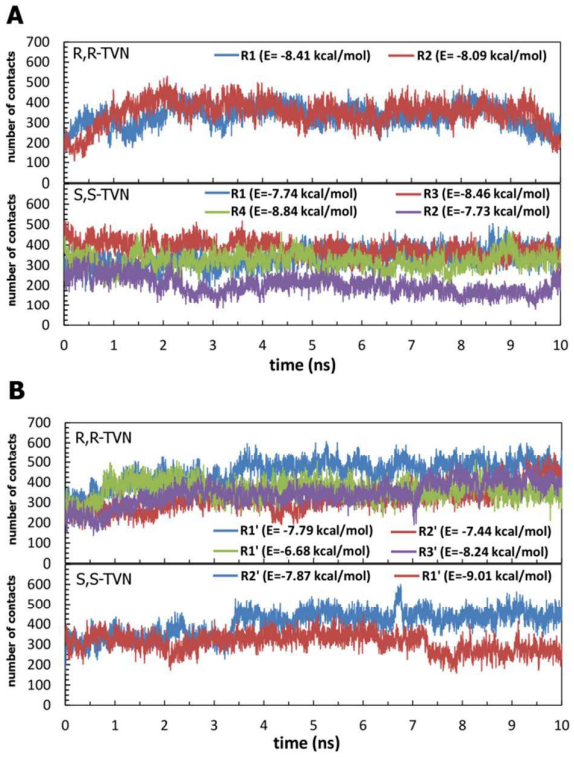

Figure 7. Stability of *trans*-δ-viniferin-Hb contacts. Number of contacts as a function of time along the MD simulations are shown for oxy- and deoxy-Hb complexes. A contact is defined if the distance between the atoms is < 4.5Å.

the pentose phosphate pathway) caused by caspase activation.

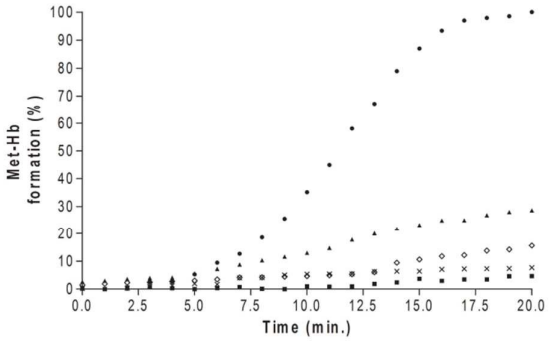

Figure 8. Time course of methemoglobin formation in the absence (circles) and presence of the racemic mixture (triangles), R,R-TVN (crosses) and S,S-TVN (rhombus) at a concentration of 50 µM. Hemolysate containing haemoglobin (3.12 mM) was treated with $NaNO_2$ 0.3 mM. Control experiments, without *trans*-δ-viniferin and under stripped conditions are also reported (squares).

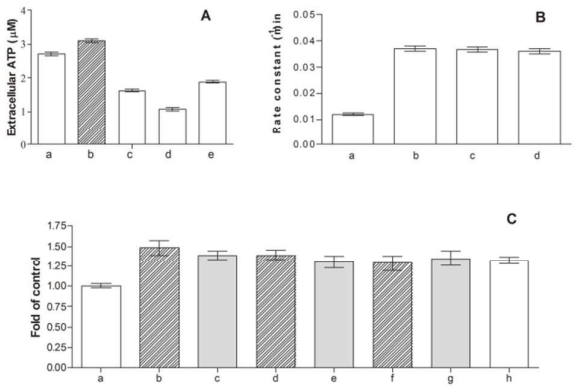

Figure 9. Effect of the racemic TVN, R,R-TVN and S,S-TVN concentrations on the ATP release (A), sulphate transport (B) and caspase activation (C) in RBCs. (A) ATP concentrations were measured at the end of the incubation time of the erythrocytes without (a) and with 4 µM Mas 7 (b), 50 µM racemic TVN (c), 50 µM R,R-TVN (d), 50 µM S,S-TVN (e). (B) Rates of sulphate transport measured in RBCs without (a) and with 50 µM of racemic TVN (b), R,R-TVN (c), S,S-TVN (d), respectively. (C) Experiments were conducted in the absence (a) or in the presence of 25 (shaded bars) and 50 (grey bars) µM of the racemic TVN (b, c), R,R-TVN (d, e), S,S-TVN (f, g), 100 µM of t-BHT (h). Results are from at least three independent experiments and expressed as mean ± standard deviation (SD).

The ATP molecule, negatively modulating the phosphofructokinase 1, key enzyme of glycolysis, would channel the glucose towards the pentose phosphate pathway with subsequent production of NADPH.

The exchange of anions (primarily HCO_3^- for Cl^-) across the erythrocyte membrane is facilitated by the human anion exchanger 1 (AE1, also called Band3).[75] We investigated the effect of the racemic TVN, R,R-TVN and S,S-TVN on Band 3-mediated anion transport in human erythrocytes to assess whether their intra-membrane localization could somehow affect trade between inside and outside of the lipid bilayer. A time course of sulphate uptake (as a measure for the level of anion transport) in human erythrocytes indicate that the sulphate influx was increased by 60% in the erythrocytes treated with racemic TVN, R,R-TVN and S,S-TVN (rate constants of 0.037 ± 0.0085 min^{-1}) when compared to controls (rate constants of 0.012 ± 0.0027 min^{-1}). The increased efficiency of anion transport is shown in Figure 9B and may be related to structural changes in band 3 and to the involvement of caspase-3.[76] In support to this hypothesis a remarkable activation of caspase-3 was observed in the presence of R,R-TVN, S,S-TVN and of the racemic TVN already at a concentration of 25 µM. In the experiments tert-butyl-hydroperoxide (t-BHT), a short-chain analogue of lipid hydroperoxides, has been used as a control (Fig. 9C). It has

been already described that oxidative stress promoted by different drugs, through a direct interaction with Hb, may lead to the activation of caspase 3, which, in turn, influences anion flux via Band 3, as well as glucose metabolism.[77]

Conclusions

We have here described the biological activity of the resveratrol derivative *trans*-δ-viniferin (TVN) and investigated the molecular basis of its interactions with hemoglobin (Hb) by means of molecular docking and dynamics calculations.

In agreement with previous studies, we have shown that, similarly to other resveratrol dimers and trimers, TVN could function as a hydroxyl radical scavenger.[12,21,52]

Notably, in the present paper we have also reported the first evaluation of the biological activities of the individual enantiomers of a resveratrol-related dimer. Using a number of assays, we have found that both enantiomers exhibit a similar but moderate biological activity. In particular, we have demonstrated that both R,R-TVN and S,S-TVN cross the erythrocyte membrane and increase the ion exchange across the membrane of the RBC, an event that is certainly positive for the physiology of the RBC as already observed for resveratrol.[59]

Here we have highlighted the binding preference of TVN for deoxy-Hb. In particular we observed higher affinity of S,S-TVN towards Hb (in comparison to R,R-TVN) which correlates with a stronger protective action exerted against oxidation caused by nitrites (Table 4). Molecular modeling studies have been further employed to provide detailed insights at atomistic level regarding the recognition of TVN by HbA. Specifically, several probable binding modes for S,S-TVN and R,R-TVN were found to exist in oxy- and deoxy-Hb, in which both H-bonding and hydrophobic contacts are important binding interactions. These findings suggest the structure-based development of novel dimers which may have a specific binding region on Hb. It should be pointed out that the approach reported here opens new possibilities for the screening and the design of resveratrol derivatives with higher antioxidant activity than the parent *trans*-resveratrol.

Acknowledgements

The authors acknowledge Regione Lombardia (Progetto SUSCHEM-Lombardia) for financial support (PG fellowship) and the National Research Council (CNR).

References

1 F. Buiarelli, F. Coccioli, R. Jasionowska, M. Merolle and A. Terracciano, *Rapid Commun. Mass Spectrom. RCM*, 2007, **21**, 2955-2964.
2 B. B. Aggarwal, A. Bhardwaj, R. S. Aggarwal, N. P. Seeram, S. Shishodia and Y. Takada, *Anticancer Res.*, 2004, **24**, 2783-2840.
3 D. Delmas, B. Jannin and N. Latruffe, *Mol. Nutr. Food Res.*, 2005, **49**, 377-395.
4 K. Szkudelska and T. Szkudelski, *Eur. J. Pharmacol.*, 2010, **635**, 1-8.
5 G. J. Soleas, E. P. Diamandis and D. M. Goldberg, *Adv. Exp. Med. Biol.*, 2001, **492**, 159-182.
6 P. Kovacic and R. Somanathan, *Oxid. Med. Cell. Longev.*, 2010, **3**, 86-100.
7 E. Tellone, M. C. De Rosa, D. Pirolli, A. Russo, B. Giardina, A. Galtieri and S. Ficarra, *Biol. Chem.*, 2014, **395**, 347-354.
8 E. Tellone, A. Galtieri, A. Russo, B. Giardina and S. Ficarra, *Oxid. Med. Cell. Longev.*, 2015, doi:10.1155/2015/392169.
9 Y. Takaya, K. Terashima, J. Ito, Y.-H. He, M. Tateoka, N. Yamaguchi and M. Niwa, *Tetrahedron*, 2005, **61**, 10285-10290.
10 P. Langcake and R. J. Pryce, *Experientia*, 1977, **33**, 151-152.
11 C. Privat, J. P. Telo, V. Bernardes-Genisson, A. Vieira, J.-P. Souchard and F. Nepveu, *J. Agric. Food Chem.*, 2002, **50**, 1213-1217.
12 H. J. Kim, E. J. Chang, S. H. Cho, S. K. Chung, H. D. Park and S. W. Choi, *Biosci. Biotechnol. Biochem.*, 2002, **66**, 1990-1993.
13 J. H. Kang, Y. H. Park, S. W. Choi, E. K. Yang and W. J. Lee, *Exp. Mol. Med.*, 2003, **35**, 467-474.
14 Y.-L. Huang, W.-J. Tsai, C.-C. Shen and C.-C. Chen, *J. Nat. Prod.*, 2005, **68**, 217-220.
15 N. Zghonda, S. Yoshida, M. Araki, M. Kusunoki, A. Mliki, A. Ghorbel and H. Miyazaki, *Biosci. Biotechnol. Biochem.*, 2011, **75**, 1259-1267.
16 R. H. Cichewicz, S. A. Kouzi and M. T. Hamann, *J. Nat. Prod.*, 2000, **63**, 29-33.
17 A.-C. Breuil, M. Adrian, N. Pirio, P. Meunier, R. Bessis and P. Jeandet, *Tetrahedron Lett.*, 1998, **39**, 537-540.
18 Y. Shikishima, Y. Takaishi, G. Honda, M. Ito, Y. Takeda, O. K. Kodzhimatov and O. Ashurmetov, *Phytochemistry*, 2001, **56**, 377-381.
19 R. Pezet, C. Perret, J. B. Jean-Denis, R. Tabacchi, K. Gindro and O. Viret, *J. Agric. Food Chem.*, 2003, **51**, 5488-5492.
20 P. Waffo-Teguo, D. Lee, M. Cuendet, J. Mérillon, J. M. Pezzuto and A. D. Kinghorn, *J. Nat. Prod.*, 2001, **64**, 136-138.
21 B.-B. Yu, X.-Z. Han and H.-X. Lou, *J. Agric. Food Chem.*, 2007, **55**, 7753–7757.
22 D. Mikulski and M. Molski, *Eur. J. Med. Chem.*, 2010, **45**, 2366-2380.
23 P. Gavezzotti, F. Bertacchi, G. Fronza, V. Křen, D. Monti and S. Riva, *Adv. Synth. Catal.*, 2015, **357**, 1831-1839.
24 E. Beneventi, S. Conte, M. R. Cramarossa, S. Riva and L. Forti, *Tetrahedron*, 2015, **71**, 3052-3058.
25 J.-K. Moon and T. Shibamoto, *J. Agric. Food Chem.*, 2009, **57**, 1655-1666.
26 P. F. Devaux, *Biochemistry (Mosc.)*, 1991, **30**, 1163-1173.
27 A. J. Schroit and R. F. A. Zwaal, *Biochim. Biophys. Acta BBA - Rev. Biomembr.*, 1991, **1071**, 313-329.
28 E. Tellone, S. Ficarra, A. Russo, E. Bellocco, D. Barreca, G. Laganà, U. Leuzzi, D. Pirolli, M. C. De Rosa, B. Giardina and A. Galtieri, *Biochimie*, 2012, **94**, 393-402.
29 D. Pirolli, B. Giardina, A. Mordente, S. Ficarra and M. C. De Rosa, *Eur. J. Med. Chem.*, 2012, **56**, 145-154.
30 A. Russo, E. Tellone, S. Ficarra, B. Giardina, E. Bellocco, G. Lagana', U. Leuzzi, A. Kotyk and A. Galtieri, *Physiol. Res. Acad. Sci. Bohemoslov.*, 2008, **57**, 49-54.
31 H. H. Dietrich, M. L. Ellsworth, R. S. Sprague and R. G. Dacey, *Am. J. Physiol. Heart Circ. Physiol.*, 2000, **278**, H1294-H1298.

32 S. Ficarra, A. Russo, F. Stefanizzi, M. Mileto, D. Barreca, E. Bellocco, G. Laganà, U. Leuzzi, B. Giardina, A. Galtieri and E. Tellone, *J. Membr. Biol.*, 2011, **242**, 31-39.
33 B. Halliwell, J. M. Gutteridge and O. I. Aruoma, *Anal. Biochem.*, 1987, **165**, 215-219.
34 A. Scala, S. Ficarra, A. Russo, D. Barreca, E. Giunta, A. Galtieri, G. Grassi and E. Tellone, *Biochim. Biophys. Acta*, 2015, **1850**, 73-79.
35 T. C. Dinis, V. M. Maderia and L. M. Almeida, *Arch. Biochem. Biophys.*, 1994, **315**, 161-169.
36 I. F. Benzie and J. J. Strain, *Anal. Biochem.*, 1996, **239**, 70-76.
37 M. S. Blois, *Nature*, 1958, **181**, 1199-1200.
38 J. Monod, J. Wyman and J.P. Changeux, *J. Mol. Biol.*, 1965, **12**, 88-118.
39 G. M. Morris, R. Huey, W. Lindstrom, M. F. Sanner, R. K. Belew, D. S. Goodsell and A. J. Olson, *J. Comput. Chem.*, 2009, **30**, 2785-2791.
40 C. Hetényi and D. van der Spoel, *FEBS Lett.,* 2006, **580**, 1447-1450.
41 D.B. Udatha, N. Sugaya, L. Olsson and G. Panagiotou, *Sci. Rep.,* 2012, **2**, 323 doi: 10.1038/srep00323.
42 A. Nakagawa, F. E. Lui, D. Wassaf, R. Yefidoff-Freedman, D. Casalena, M. A. Palmer, J. Meadows, A. Mozzarelli, L. Ronda, O. Abdulmalik, K. D. Bloch, M. K. Safo and W. M. Zapol, *ACS Chem. Biol.*, 2014, **9**, 2318-2325.
43 G.M. Morris, R. Huey, W. Lindstrom, M.F. Sanner, R.K. Belew, D.S. Goodsell and A.J. Olson, *J. Comput. Chem.,* 2009, **16**, 2785-2791.
44 T. Klabunde, H. M. Petrassi, V. B. Oza, P. Raman, J. W. Kelly and J. C. Sacchettini, *Nat. Struct. Biol.*, 2000, **7**, 312-321.
45 A. D. Mackerell, M. Feig and C. L. Brooks, *J. Comput. Chem.*, 2004, **25**, 1400-1415.
46 S.-Y. Park, T. Yokoyama, N. Shibayama, Y. Shiro and J. R. H. Tame, *J. Mol. Biol.*, 2006, **360**, 690-701.
47 R. A. Friesner, J. L. Banks, R. B. Murphy, T. A. Halgren, J. J. Klicic, D. T. Mainz, M. P. Repasky, E. H. Knoll, M. Shelley, J. K. Perry, D. E. Shaw, P. Francis and P. S. Shenkin, *J. Med. Chem.*, 2004, **47**, 1739-1749.
48 B. Hess, C. Kutzner, D. van der Spoel and E. Lindahl, *J. Chem. Theory Comput.*, 2008, **4**, 435-447.
49 C. Oostenbrink, A. Villa, A. E. Mark and W. F. van Gunsteren, *J. Comput. Chem.*, 2004, **25**, 1656-1676.
50 T. Darden, L. Perera, L. Li and L. Pedersen, *Structure*, 1999, **7**, R55-R60.
51 B. Hess, *J. Chem. Theory Comput.*, 2008, **4**, 116-122.
52 H. J. Kim, E. J. Chang, S. H. Cho, S. K. Chung, H. D. Park and S. W. Choi, *Biosci. Biotechnol. Biochem.*, 2002, **66**, 1990-1993.
53 B. Halliwell and J. M. Gutteridge, *Arch. Biochem. Biophys.*, 1986, **246**, 501-514.
54 E. Niki and N. Noguchi, *IUBMB Life*, 2000, **50**, 323-329.
55 E. Niki and N. Noguchi, *Acc. Chem. Res.*, 2004, **37**, 45-51.
56 E. Niki, Y. Omata, A. Fukuhara, Y. Saito and Y. Yoshida, *J. Agric. Food Chem.*, 2008, **56**, 8255-8260.
57 L. A. Stivala, M. Savio, F. Carafoli, P. Perucca, L. Bianchi, G. Maga, L. Forti, U. M. Pagnoni, A. Albini, E. Prosperi and V. Vannini, *J. Biol. Chem.*, 2001, **276**, 22586-22594.
58 İ. Gülçin, *Innov. Food Sci. Emerg. Technol.*, 2010, **11**, 210-218.
59 A. Galtieri, E. Tellone, S. Ficarra, A. Russo, E. Bellocco, D. Barreca, R. Scatena, G. Laganà, U. Leuzzi and B. Giardina, *Biol. Chem.*, 2010, **391**, 1057-1065.
60 A. Lançon, D. Delmas, H. Osman, J.P. Thénot, B. Jannin and N. Latruffe, *Biochem. Biophys. Res. Commun.,* 2004, **316**, 1132-1137.
61 J. M. Rifkind and E. Nagababu, *Antioxid. Redox Signal.*, 2013, **18**, 2274-2283.
62 P.H. Hinderling, *Pharmacol. Rev.,* 1997, **49**, 279-295.
63 C. Hetényi and D. van der Spoel, *Protein Sci.*, 2009, **11**, 1729-1737.
64 H.J. Hocker, K.J. Cho, C.Y. Chen, N. Rambahal, S.R. Sagineedu, K. Shaari, J. Stanslas, J.F. Hancock and A.A. Gorfe, *Proc. Natl. Acad. Sci. USA*, 2013, **110,** 10201-10206.
65 P. Källblad, R. L. Mancera and N. P. Todorov, *J. Med. Chem.*, 2004, **47**, 3334-3337.
66 D. Kozakov, K. H. Clodfelter, S. Vajda and C. J. Camacho, *Biophys. J.*, 2005, **89**, 867-875.
67 A. C. Wallace, R. A. Laskowski and J. M. Thornton, *Protein Eng.*, 1995, **8**, 127-134.
68 W. J. Wallace, R. A. Houtchens, J. C. Maxwell and W. S. Caughey, *J. Biol. Chem.*, 1982, **257**, 4966-4977.
69 M. C. Kohn, *Drug Metab. Dispos.*, 2002, **30**, 676-683.
70 A. Tomoda, Y. Yoneyama and A. Tsuji, *Biochem. J.*, 1981, **195**, 485-492.
71 J. E. Jagger, R. M. Bateman, M. L. Ellsworth and C. G. Ellis, *Am. J. Physiol. Heart Circ. Physiol.*, 2001, **280**, H2833-H2839.
72 W. Subasinghe and D. M. Spence, *Anal. Chim. Acta*, 2008, **618**, 227-233.
73 M. L. Ellsworth, C. G. Ellis, D. Goldman, A. H. Stephenson, H. H. Dietrich and R. S. Sprague, *Physiology*, 2009, **24**, 107-116.
74 A. M. Forsyth, J. Wan, W. D. Ristenpart and H. A. Stone, *Microvasc. Res.*, 2010, **80**, 37-43.
75 M. J. Tanner, *Mol. Membr. Biol.*, 1997, **14**, 155-165.
76 D. Mandal, V. Baudin-Creuza, A. Bhattacharyya, S. Pathak, J. Delaunay, M. Kundu and J. Basu, *J. Biol. Chem.*, 2003, **278**, 52551-52558.
77 E. Tellone, S. Ficarra, B. Giardina, R. Scatena, A. Russo, M. E. Clementi, F. Misiti, E. Bellocco and A. Galtieri, *J. Membr. Biol.*, 2008, **224**, 1-8.